Structural and electronic properties of Fe^{3+} and Fe^{2+} centers in GaN from optical and EPR experiments

E. Malguth,* A. Hoffmann, and W. Gehlhoff
Institut für Festkörperphysik, Technische Universität Berlin, Hardenbergstraße 36, 10623 Berlin, Germany

O. Gelhausen and M. R. Phillips
Microstructural Analysis Unit, University of Technology, Sydney, Broadway, NSW 2007 Australia

X. Xu†
Cree, Inc., 4600 Silicon Drive, Durham, North Carolina 27703, USA

(Received 26 May 2006; revised manuscript received 11 August 2006; published 3 October 2006)

This work provides a consistent picture of the structural, optical, and electronic properties of Fe-doped GaN. A set of high-quality GaN crystals doped with Fe at concentrations ranging from 5×10^{17} cm^{-3} to 2×10^{20} cm^{-3} is systematically investigated by means of electron paramagnetic resonance and various optical techniques. Fe^{3+} is shown to be a stable charge state at concentrations from 1×10^{18} cm^{-3}. The fine structure of its midgap states is successfully established, including an effective-mass-like state consisting of a hole bound to Fe^{2+} with a binding energy of 50 ± 10 meV. A major excitation mechanism of the $Fe^{3+}({}^4T_1\rightarrow{}^6A_1)$ luminescence is identified to be the capture of free holes by Fe^{2+} centers. The holes are generated in a two-step process via the intrinsic defects involved in the yellow luminescence. The $Fe^{3+/2+}$ charge-transfer level is found 2.863 ± 0.005 eV above the valence band, suggesting that the internal reference rule does not hold for the prediction of band offsets of heterojunctions between GaN and other III-V materials. The $Fe^{2+}({}^5E\rightarrow{}^5T_2)$ transition is observed around 390 meV at any studied Fe concentration by means of Fourier transform infrared spectroscopy. Charge-transfer processes and the effective-mass-like state involving both Fe^{2+} states are observed. At Fe concentrations from 1×10^{19} cm^{-3}, additional lines occur in electron paramagnetic resonance and photoluminescence spectra which are attributed to defect complexes involving Fe^{3+}. With increasing Fe concentration, the Fermi level is shown to move from near the conduction band to the $Fe^{3+/2+}$ charge-transfer level, where it stays pinned for concentrations from 1×10^{19} cm^{-3}. Contrary to cubic II-VI and III-V materials, both electronic states are effected by only a weak Jahn-Teller interaction.

DOI: 10.1103/PhysRevB.74.165202 PACS number(s): 71.55.Eq, 71.20.Be, 71.55.−i, 71.70.Ch

I. INTRODUCTION

Acting as a deep acceptor, iron is currently introduced into GaN to compensate inherent *n*-type conductivity and to produce semi-insulating substrate material necessary for the production of high-performance GaN/AlGaN high-electron-mobility transistors.[1–3] Moreover, Fe-doped GaN is widely considered to be a potential material to realize future spintronic applications. However, the impact of Fe on the optical, electrical, and magnetic properties of GaN is not well understood, and hence they cannot be sufficiently controlled at present. In particular for spintronic applications, a detailed knowledge of the occurring charge states and their respective electronic structure is crucial to model carrier-mediated ferromagnetism.[4,5] Of great importance is knowledge of the exact position of the $Fe^{3+/2+}$ acceptor level within the band gap because it is used to predict band offsets in heterostructures on the basis of the internal reference rule.[6,7] Furthermore, the behavior of d^5 and d^6 systems in a trigonal crystal field of C_{3V} symmetry is of general physical interest for aspects of group and crystal-field theory.

In GaN with a wurtzite lattice type, the Ga site has a tetrahedral symmetry that is axially distorted along the *c* axis, resulting in C_{3V} symmetry. To a good approximation, the crystal field can be considered to be equivalent to the perfect tetrahedral T_d symmetry present in cubic crystals (zinc blende). The impact of the ligand field in form of a Stark effect causes the d^5 configuration of Fe^{3+} on Ga site to split into the ground state ${}^6A_1(S)$ and the excited states ${}^4T_1(G)$, ${}^4T_2(G)$, and ${}^4E(G)$.[8] The spin-forbidden ${}^4T_1(G)\rightarrow{}^6A_1(S)$ transition is observed as an IR luminescence at 1.299 eV with a lifetime of 8 ms and has been unequivocally assigned by Zeeman experiments.[9–11] Spin and parity selection rules are relaxed under the influence of the C_{3V} crystal field, and lattice strain can shift the emission line by ~1 meV.[10] Three further lines are reported to appear at higher temperatures, reflecting the fine structure of the ${}^4T_1(G)$ state.[10,11] Heitz *et al.* found the higher excited states ${}^4T_2(G)$ and ${}^4E(G)$ at 2.01 and 2.731 eV above the ground state, respectively, and also identified an exciton bound to the Fe center constituting a shallow acceptor state (Fe^{3+},e,h) at 2.888 eV above the ground state.[8] Based on the established position of the $Fe^{3+/2+}$ charge-transfer (CT) level at 3.17 eV above the valence band (VB) the following conclusions were drawn by these workers: (i) The binding energy of the bound state is 280 meV, (ii) the $Fe^{2+}({}^5T_2)$ state is degenerated with the conduction band (CB), and (iii) the internal reference rule fails for GaN in conjunction with other III-V materials, including nitrides.[6–8]

The ${}^5D$ ground state of the Fe^{2+} center of the d^6 configuration splits into the states ${}^5E$ and ${}^5T_2$ under the influence of the ligand field. While the transition between these two has

TABLE I. Resistivity of Fe-doped GaN samples measured by ATMI at room temperature.

Fe concentration (cm^{-3})	Resistivity (Ω cm)
5×10^{17}	200
1×10^{18}	1×10^{8}
1×10^{19}	3×10^{8}
2×10^{20}	900

been reported for cubic III-V materials, it is believed to be absent in GaN.[12]

In this work, we present a systematic study of the physical properties of Fe-doped GaN with a particular focus on the electronic structure of the detected 3+ and 2+ charge states. The fine structure of all observed Fe^{3+} states is established, while a forthcoming paper is dedicated to the fine structure of the Fe^{2+} states ^5E and $^5T_2$.[13] High-quality samples have facilitated precise determination of the Fe-related energy states in GaN:Fe. Major corrections of the previously reported bound state and the energy position of the $Fe^{3+/2+}$ CT level are also made. Finally, we report the presence of the $Fe^{2+}(^5E\rightarrow{}^5T_2)$ transition in GaN. A comprehensive picture of the electronic properties of Fe centers in GaN is developed by studying GaN with varying Fe concentration using a broad array of spectroscopies, including electron paramagnetic resonance (EPR), photoluminescence (PL), transmission spectroscopy, PL excitation (PLE), and Fourier transform infrared spectroscopy (FTIR).

II. EXPERIMENTAL DETAILS

A set of Fe-doped GaN samples grown by the company ATMI using hydride vapor phase epitaxy (HVPE) on sapphire substrate was investigated in this work. The epilayers had a wurtzite crystal structure with their *c* axis aligned to the growth direction. Iron was incorporated during the growth process at concentrations ranging from 5×10^{17} cm^{-3} to 2×10^{20} cm^{-3} as determined by secondary ion mass spectroscopy. The substrate was removed resulting in ~400-μm-thick freestanding samples which were cut into pieces of approximately (2×2) mm^2. These samples facilitated optical experiments with the light traveling perpendicular to the *c* axis, providing enhanced absorption and polarized spectroscopy measurements. The sample resistivities are presented in Table I.

For PL experiments and transmission spectroscopy in the ultraviolet to visible (UV-VIS) spectral region, the samples were kept in liquid helium at a temperature of 1.8 K with the *c* axis perpendicular to the optical path. PL was excited by the 2.412-eV line of an Ar-ion laser. The emitted light was passed through a polarizer and dispersed by a 1-m Spex double monochromator and detected by a nitrogen-cooled Ge detector. For UV-VIS transmission spectroscopy, depending on the spectral region, a xenon lamp or halogen-tungsten lamp in combination with a polarizer served as light source. The transmitted light was dispersed by a 1-m Jarrel-Ash monochromator and detected by a photomultiplier based on a bialkali metal, GaAs or Ge. FTIR transmission measurements were carried out using the IFS 66v spectrometer from Bruker with a globar, KBr beam splitter and HgCdTe-based detector. The samples were cooled to 50 K by a liquid-helium contact cryostat with KBr windows. In PLE experiments, the samples were cooled down to 7 K. A halogen lamp in combination with a 275-mm double monochromator served as tunable light source, providing a resolution of 5 meV. A 300-mm double monochromator with the same resolution was used in detection. The EPR measurements were carried out using a Bruker ESP 300E spectrometer operating at the *X* band (≅9.5 GHz). A temperature of 4 K was achieved with an Oxford Instruments continuous-flow cryostat.

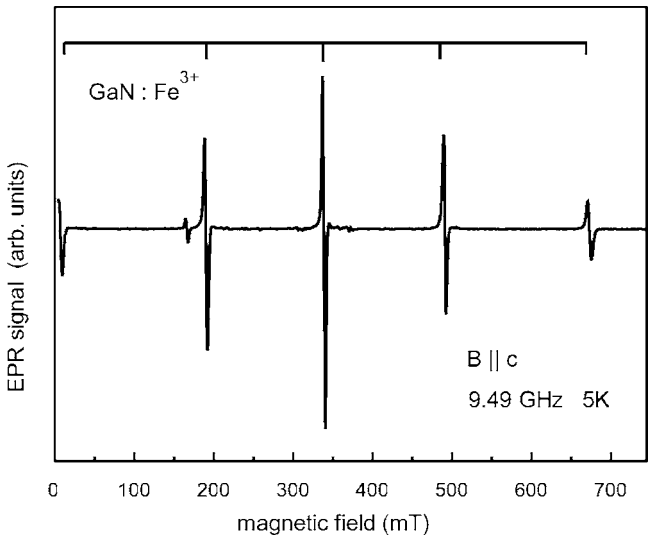

FIG. 1. *X*-band EPR spectrum of Fe-doped GaN with a Fe concentration of 1×10^{19} cm^{-3} at 4 K for $B\|c$ axis. The line positions of the five allowed fine-structure transitions ($\Delta M=\pm1$) are indicated.

III. RESULTS AND DISCUSSION

In this section, first, the influence of Fe doping on the crystalline quality and the electrical properties of GaN is discussed. Second, high-resolution optical studies by PL, PLE, and transmission spectroscopy were performed to understand the nature of the Fe^{3+} and the Fe^{2+} centers in GaN.

A. Fe^{3+} center

1. Structural quality

The structural quality of the Fe-doped GaN samples was analyzed by EPR measurements. In Fig. 1, an EPR spectrum ($B\|c$ axis) for an Fe-doped GaN sample with an Fe concentration of 1×10^{19} cm^{-3} is depicted. It displays five sharp fine-structure transitions that are typical for an $S=\frac{5}{2}$ ion in axial (C_{3V}) symmetry and are unambiguously assigned to the d^5 configuration of the Fe^{3+} center on Ga site. The lines belong to the transitions $\left(-\frac{1}{2}\leftrightarrow\pm\frac{1}{2}\right)$, $\left(\pm\frac{3}{2}\leftrightarrow\pm\frac{1}{2}\right)$, and

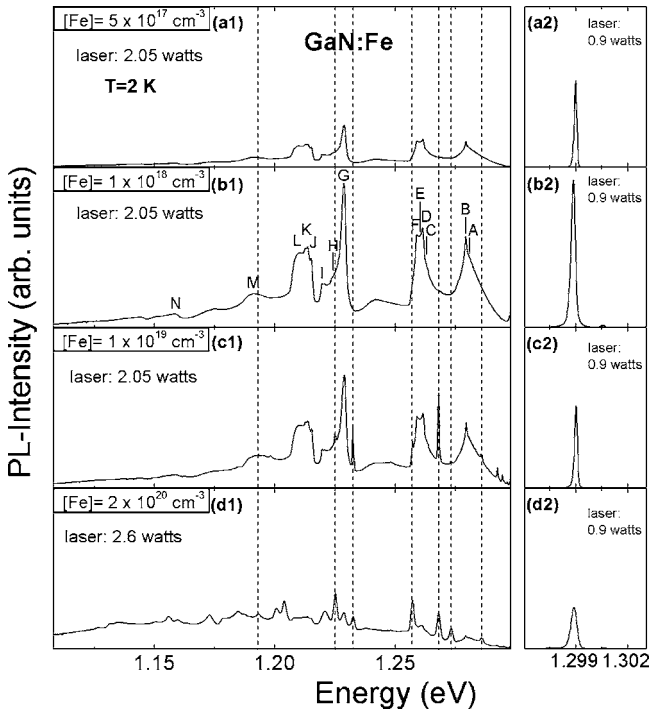

FIG. 2. Low-temperature (2-K) luminescence of the Fe^{3+} ($^4T_1(G) \rightarrow {}^6A_1(S)$) transition in GaN for different Fe concentrations. Excitation at 2.412 eV. Stated laser intensity is output power. The dominating zero-phonon line (ZPL) at 1.299 eV is displayed at a different energy scale for better resolution. All spectra are displayed on the same intensity scale for quantitative comparison. ZPL's developing with increasing Fe concentration due to the formation of Fe complexes are indicated by dashed lines. Capital letters in spectrum (b1) indicate vibrational replicas that are identified in Table II.

$\left(\pm\frac{5}{2} \leftrightarrow \pm\frac{3}{2}\right)$ with $\Delta M = \pm 1$ (in the order of decreasing intensity). Compared with previous studies,[9] the samples investigated in this work are of much higher crystal quality and do not exhibit a random strain broadening. This fact is supported by the sharpness of the outer line pairs of fine-structure transitions $\left(\pm\frac{5}{2} \leftrightarrow \pm\frac{3}{2}\right)$, which indicates that the Fe centers are incorporated relatively strain free. A similar high quality EPR spectrum is observed at 300 K as well. Due to the high Debye temperature of GaN (600 K), spin-lattice relaxation does not result in excessive EPR line broadening at room temperature.[14] In connection with additional EPR measurements in the Q band (34 GHz), the smaller linewidths seen in Fig. 1 allow one to determine the spin Hamiltonian parameters more accurately than in previous works.[15]

Other Fe charge states than Fe^{3+} were not detected by EPR experiments.

2. [$^4T_1(G)$-$^6A_1(S)$] *transition*

Near-infrared PL spectra of Fe-doped GaN are shown Fig. 2 for various Fe concentrations. The typical Fe^{3+} ($^4T_1(G) \rightarrow {}^6A_1(S)$) transition with a vibrational sideband is observed at any investigated Fe concentration. The position and the full width at half maximum (FWHM) of the zero-phonon line (ZPL) as a function of the Fe concentration are displayed in Figs. 5(a) and 5(b), respectively, below. The observed FWHM which is as low as 120 μeV confirms the good crystal quality and strain-free incorporation of iron as suggested by EPR measurements. The increasing FWHM with rising Fe concentration is probably due to the modified crystal field caused by the substitution of Ga by Fe ions which is only felt by neighboring Fe centers at high Fe densities. The concentration of Fe^{3+} centers is expected to scale with the overall iron content due to the shift of the Fermi level discussed above. However, the intensity of the Fe^{3+}-related luminescence observed herein is independent of the Fe concentration. Incomplete excitation of the Fe^{3+} due to an insufficient laser intensity is quite unlikely to account for this observation because of the long lifetime (8 ms) of the spin-forbidden transition.[11] Consequently, an extra-center excitation process, which is still to be identified, must be the bottleneck.

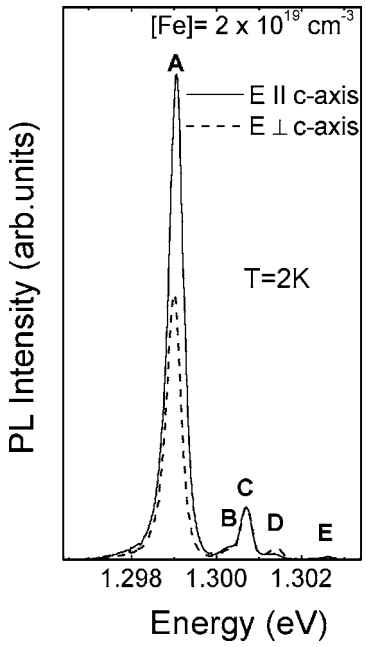

FIG. 3. Polarized high-resolution PL spectra of the $^4T_1(G) \rightarrow {}^6A_1(S)$ ZPL of Fe^{3+} in GaN at $T=2$ K, [Fe]$=1\times10^{19}$ cm^{-3}. At an excitation power of 4 W (output), transitions involving higher $^4T_1(G)$ sublevels appear on the high-energy side of the ZPL at 1.299 eV.

3. *Excited* $^4T_1(G)$ *state*

A closer investigation of the ZPL of the sample with an Fe concentration of 1×10^{19} cm^{-3} at an increased excitation intensity is presented in Fig. 3. Additional lines on the high-energy side can be observed 1.10, 1.72, 2.42, and 3.65 meV above the ZPL at 1.299 eV. The latter three lines have been observed before in experiments at 10 K.[10,11]

The $^6A_1(S)$ state of Fe^{3+} splits, due to the spin-orbit coupling, into states of Γ_7 and Γ_8 symmetry separated by only 90 μeV, which is negligible compared with the linewidth. Therefore, the additional peaks represent transitions starting at excited $^4T_1(G)$ sublevels. The exact fine structure of the $^4T_1(G)$ state is the result of spin-orbit coupling and the Jahn-Teller effect as well as the axial distortion of the trigonal

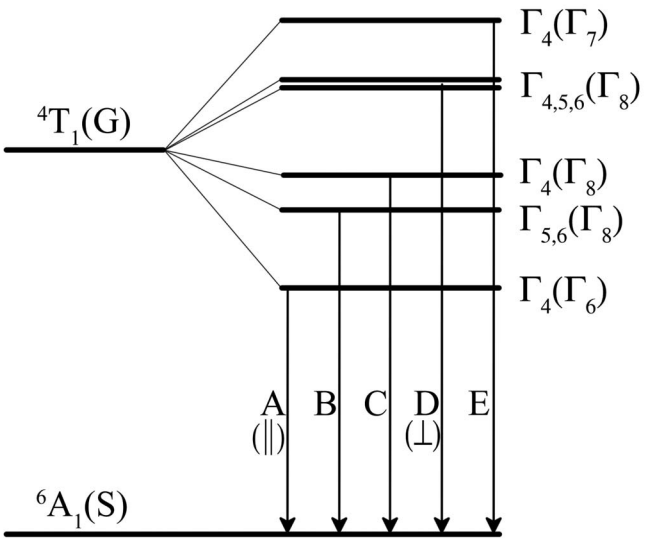

FIG. 4. Splitting of the $^4T_1(G)$ state in trigonal C_{3V} symmetry, derived from the fine structure of the $^4T_1(G) \rightarrow {}^6A_1(S)$ luminescence (Fig. 3). The original symmetries resulting from only spin-orbit coupling are given in brackets. Observed transitions and their respective polarization are indicated by arrows. Letters refer to the PL spectrum, Fig. 3.

crystal field in C_{3V} symmetry of the wurtzite lattice structure. The spin-orbit interaction causes a splitting into four states of Γ_6, Γ_8, Γ_7, and Γ_8 symmetry. In cubic II-VI and III-V crystals a strong Jahn-Teller effect involving *E*-type phonon modes quenches the orbital momentum, reducing the fourfold splitting to a doublet with a splitting of about 1 meV.[16–18] However, the fivefold splitting of about 4 meV observed in Fig. 3 indicates only a weak or intermediate Jahn-Teller interaction. The lower defect symmetry in wurtzite structure stabilizes the Fe^{3+} center against the Jahn-Teller coupling as has been established for the $^4T_1(G)$ state in ZnO.[19] Moreover, a splitting of at least one spin-orbit state in C_{3V} symmetry needs to be taken into account to understand the fivefold splitting. It should be noted that the first peak above the ZPL (1.1 meV) is the smallest. This observation suggests that a selection rule is softened by the C_{3V} crystal field causing the second most populated state to exhibit the lowest intensity.

The observed polarization of each emission line in Fig. 3 allows us to tentatively assign them to $^4T_1(G)$ substates and, consequently, to derive the fine structure of the $^4T_1(G)$ state in C_{3V} crystal-field symmetry. The result is depicted in Fig. 4. As mentioned above, spin-orbit coupling results in four states of Γ_6, Γ_8, Γ_7, and Γ_8 symmetry (see brackets in Fig. 4) which under the impact of axial distortion (C_{3V} symmetry) of the crystal field transform as follows:

$$\Gamma_6 \rightarrow \Gamma_4,$$

$$\Gamma_7 \rightarrow \Gamma_4,$$

$$\Gamma_8 \rightarrow \Gamma_4, \Gamma_5, \Gamma_6,$$

removing the degeneracy of the Γ_8 states. Only the splitting of the lower Γ_8 state is resolved. In comparison to the Fe^{3+} ($^4T_1(G)$) state in ZnO, the energetic positions of the top spin-orbit states (Γ_7 and Γ_8) are swapped[19] because the trigonal crystal field is stretched in ZnO, while it is compressed in GaN. The observed 4 meV splitting of the $^4T_1(G)$ state is consistent with the same state in ZnO.[19]

4. Vibrational modes

The sideband of the Fe^{3+} ($^4T_1(G) \rightarrow {}^6A_1(S)$) luminescence, which is displayed in Figs. 2(a1), (b1), (c1), and (d1), is a superposition of vibrational replica of the ZPL at 1.299 eV and additional sharp lines (FWHM=400 μeV), which are marked by dashed lines. The latter are only present for Fe concentrations above 1×10^{19} cm^{-3} [Figs. 2(c1) and 2(d1)], while the spectra of Figs. 2(a1) and 2(b1) consist of only the local vibrational modes (LVMs) and phonon modes.[9,11] In this spectral region, in previous studies of the Fe^{3+} center, further lines were observed which could be successfully assigned to the presence of other transitions-metal centers such as V^{3+}, Cr^{4+}, Ti^{2+}, or Co^{2+}.[8–10,20–23] The absence of those lines in our spectra suggests that our Fe-doped GaN samples are of high purity.

For a detailed analysis of the vibronic coupling of the Fe^{3+} center, the replicas observed for low Fe concentrations [Fig. 2(b1)] are compiled in Table II including their favored polarization (polarized spectra not shown). Their energies are compared to phonon modes of the host lattice[24,25] and to LVMs.[26,27] We observe a strong coupling on E_2 phonon modes and A_1 and *E* LVMs. The nature of the very strong replica at 19.8 meV, which has been detected before and interpreted as the actual E_2(low) phonon,[22] is still unclear.

The energy of the E_2 phonon mode is sensitive to lattice strain.[28] Therefore, measuring the energetic distance between the ZPL and an E_2 replica provides a way to probe the local strain induced by the iron incorporation. The energy of the E_2(high) phonon mode remains constant (70.1 meV) with varying Fe concentration [Fig. 5(c)], confirming the relatively stress-free incorporation of iron, even for concentrations as high as 2×10^{20} cm^{-3}. This result was confirmed by determining the energy of the E_2(high) phonon mode using Raman scattering (measurements not shown).

5. Fe^{3+}-related complexes

The additional sharp lines which appear within the sideband for high Fe concentrations [Figs. 2(c1) and 2(d1)] have been observed before and were attributed to the formation of defect complexes involving iron.[8,14,29] This assignment is supported by the fact that the intensity of the lines in question scales with the Fe concentration. Figure 6 shows the spectrum of only the additional lines. It was derived by subtracting the phonon and LVM spectrum, Fig. 2(a1), from the sideband including the defect lines, Fig. 2(c1).

The most pronounced line at 1.268 eV with a FWHM of 580 μeV is attributed to a complex involving a donor (Fe^{3+}, D^+) on the basis of PLE spectra which can be explained with the Fe^{3+}-term scheme considering the presence of additional excitation mechanisms.[29] Further similarities to the luminescence of the isolated Fe^{3+} center are a long lifetime indicating a spin-forbidden transition and the observation of higher

TABLE II. Sideband of $Fe^{3+}({}^4T_1(G)\text{-}{}^6A_1(S))$ luminescence. Listed are the replicas as seen for [Fe]=5 $\times 10^{18}$ cm^{-3} in Fig. 2(b1) and their favored polarization. ΔE is the energetic distance from the ZPL at 1.299 eV. Moreover, possible phonon modes (Refs. 24 and 25) and LVMs (Refs. 26 and 27), including their energies are given in the last three columns.

Line	E (eV)	ΔE (meV)	Polarization	$\hbar\omega$ (meV)	Vibrational mode	Ref.
A	1.28110	17.9		17.80	E_2(low)	24
B	1.27920	19.8				
C	1.26290	36.1		*A*+*A*		
D	1.26150	37.5		37.30	LVM (A_1)	26
E	1.25980	39.2	∥	39.20	LVM (A_1)	26
F	1.25910	39.9	∥	39.55	B_1(low)	25
G	1.22890	70.1	⊥	70.50	E_2(high)	24
H	1.22415	74.8	⊥	*D*+*D* or 75.10	LVM A_1	27
I	1.21960	79.4	⊥			
J	1.21520	83.8	∥			
K	1.21380	85.2	⊥	85.50	LVM (A_1)	26
L	1.20995	89.0		88.90	LVM (*E*)	26
M	1.19140	107.6		*D*+*G*		
N	1.15830	140.7		*G*+*G*		

levels of the excited state at high temperatures.[29] However, a strongly modified electronic structure is suggested by the Zeeman behavior not showing the fingerprint of a d^5 configuration.[29]

Table III summarizes lines of higher energies and points out possible vibronic replicas of the 1.268-eV line. This association is supported by identical PLE spectra at least for the lines at 1.2324 and 1.1933 eV. Basically, a coupling with the same phonon and local vibrational modes as for the 1.299-eV line is observed. Differences particularly regarding the LVM energies are plausible as the neighborhood of the Fe^{3+} center as part of a complex differs from that of the isolated Fe^{3+} center. It should be noted that the replica at 1.193 eV is found at the same position as the Cr^{4+} luminescence in GaN specimens of poorer purity.[23]

Further lines in Fig. 6 must be ZPL's themselves or replicas of one. Obviously, iron forms different complexes with other defects. Their exact nature still remains unclear. As mentioned above, complexes involving donors—e.g., nitrogen vacancies or oxygen—have been suggested as the origin of the additional lines under discussion.[14,29] However, that does not quite explain the strong dependence on the Fe concentration. From this perspective Fe-Fe complexes are more plausible.

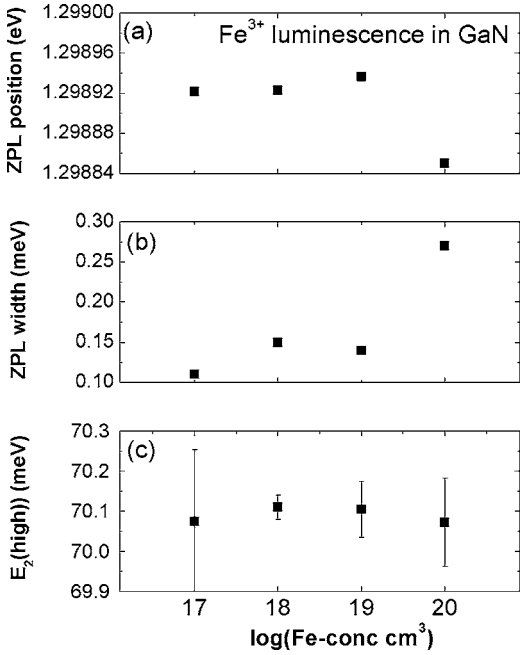

FIG. 5. Concentration dependence of the $Fe^{3+}({}^4T_1(G)\text{-}{}^6A_1(S))$ luminescence: (a) position of the ZPL, (b) FWHM of ZPL, and (c) energy of the *E*2 phonon mode.

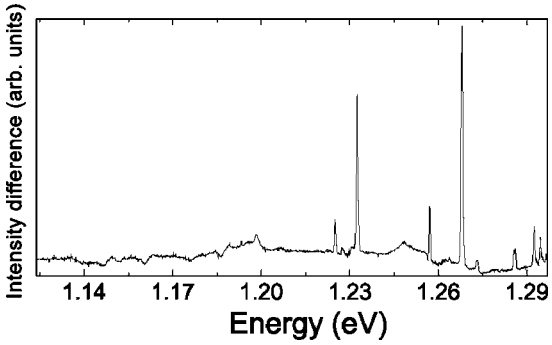

FIG. 6. PL difference spectrum of the sideband of the Fe^{3+} emission in GaN. In Fig. 2 the spectrum (a1) was subtracted from spectrum (c1), revealing the Fe-complex lines.

TABLE III. Sharp lines associated with Fe complexes and their polarization. Only the ZPL at 1.268 eV and lines at smaller energies are listed. Possible phonon modes (Ref. 24) and LVMs (Ref. 26) are given in the last column including their energies.

Line (eV)	Polarization	ΔE (meV)	$\hbar\omega^2$	Vibrational mode
1.2681	$\perp$			
1.2638		4.3		
1.2571	$\parallel$	11.0		
1.2483		19.8		
1.2324	$\perp$	35.7	37.3	LVM (A_1)
1.2250	$\parallel$	43.1	39.2	LVM (E)
1.1983		69.8	70.50	E_2(high)
1.1933		74.8	$2\times37,3$	

An additional fingerprint of Fe^{3+}-related defect complexes in heavily Fe-doped GaN comes from angular-dependent EPR spectra, as illustrated in Fig. 7. The dominant lines with strong intensity originate from allowed transitions ($\Delta M=\pm1$) of isolated Fe^{3+} centers. Also, due to the relatively large zero-field splitting of $D=-0.0768$ cm^{-3} and the corresponding strong mixing of wave functions, several forbidden transitions ($\Delta M=\pm2,\pm3,\pm4,\pm5$) of lower intensity are observed. A characteristic of forbidden transitions is the vanishing of the respective lines in the main crystal directions—i.e., $B\|c$ axis or $B\perp c$ axis—as shown in Fig. 7. The theoretically calculated angular dependences of the EPR peaks are indicated in Fig. 7 by solid (allowed transitions) and dashed (forbidden transitions) lines. Apart from the lines attributed to isolated Fe^{3+} centers, additional weak transitions are detected, which support the optical observation of Fe^{3+}-related defect complexes. Most of these lines appear as

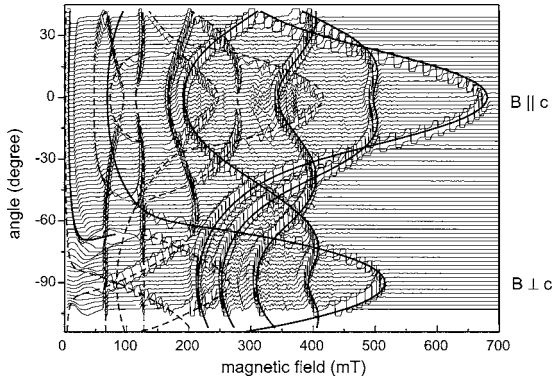

FIG. 7. EPR spectra of Fe-doped GaN, [Fe]$=1\times10^{19}$ cm^{-3}, 9.49 GHz, and 4 K. Stack plot for rotation of the magnetic field (5° step width) from $B\|c$ axis to $B\perp c$ axis. In this graph, the five allowed transitions ($\Delta M=\pm1$) of Fe^{3+} with $S=\frac{5}{2}$ are observed with strong intensity, while the forbidden transitions ($\Delta M=\pm2,\pm3,\pm4,\pm5$) appear as weak resonances. Theoretical line positions were calculated for allowed (solid curve) and forbidden (dashed curve) transitions using the corresponding spin Hamiltonian for Fe^{3+} in GaN and the parameters given in Ref. 15. Additional weak transitions mainly originate from Fe^{3+}-Ga pairs.

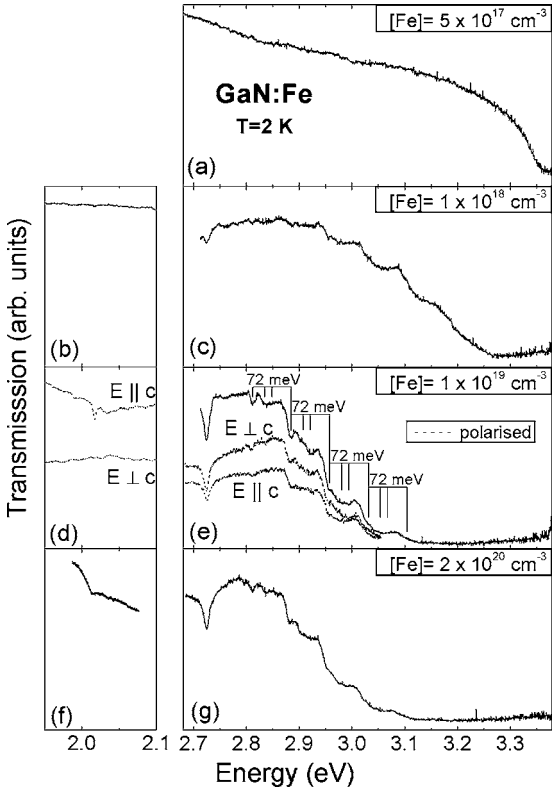

FIG. 8. Optical transmission spectra of Fe-doped GaN with different concentrations of iron at 2 K using a xenon lamp. Irradiating perpendicular to the c axis the path length through the sample was ~2 mm. Polarized measurements are only presented for an iron content of 1×10^{19} cm^{-3}. The steplike structure associated with the effective-mass-like state at 2.812 eV is indicated for [Fe]$=1\times10^{19}$ cm^{-3}.

weak satellites of the dominant Fe^{3+} transitions and are attributed to $Fe_{Ga}{}^{3+}$-Ga_i pairs.[30] In wurtzite lattice structure, there are 12 possible center orientations of these pairs leading to the observed multitude of lines. The most prominent of those lines originate from centers with the principal axis nearly in parallel with the c axis and are analyzed in Ref. 30. $Fe_{Ga}{}^{3+}$-Ga_i pairs are potential candidates for the additional luminescence lines in Figs. 2(c1) and 2(d1). However, other complexes that are undetectable by EPR cannot be ruled out in this context. A few very weak lines in Fig. 7 cannot be attributed to $Fe_{Ga}{}^{3+}$-Ga_i pairs and might in fact originate from Fe-Fe pairs.

6. Higher excited states: $^4T_2(G)$ and $^4E(G)$

The transmission spectra in Fig. 8 reveal higher excited Fe^{3+} states for Fe concentrations from 1×10^{18} cm^{-3}. The main absorption features are compiled and assigned in Table IV. Transitions into the excited Fe^{3+} states $^4T_2(G)$ and $^4E(G)$ appear as peaks at 2.0172 eV and 2.7247 eV, respectively.[8] The observed weak phonon coupling is typical for intracenter transitions.[31] The relatively large FWHM of 2.8 meV and 7.4 meV (for [Fe]$=\times10^{19}$ cm^{-3}), respectively, are natural and not due to limited spectral resolution. The $^4T_2(G)$-$^6A_1(S)$ absorption [Fig. 8(d)] exhibits a pronounced polariza-

TABLE IV. Absorption lines found in UV-VIS transmission spectra at 2 K with the polarization given in brackets. ΔE refers to the last value of the group above. Possible assignments are given in the right column.

Absorption line (eV)	ΔE (meV)	Assignment
2.0172 (∥)		$^4T_2(G)$-$^6A_1(S)$
2.7247		$^4E(G)$-$^6A_1(S)$
2.7244 (⊥)	−0,3	$^4E(G)$-$^6A_1(S)$
2.7258 (∥)	1,1	$^4E(G)$-$^6A_1(S)$
2.812	87	ZPL of (Fe^{2+},h)-$^6A_1(S)$
2.836	24	
2.849	37	LVM (A_1) of ZPL
2.884	72	E_2(high) or LVM A_1
2.908	24	
2.922	38	$(E_2$ or $A_1)+A_1$
2.957	73	$2(E_2$ or $A_1)$
2.981	24	
2.995	38	$2(E_2$ or $A_1)+A_1$
3.030	73	$3(E_2$ or $A_1)$

tion ($E \| c$ axis). Polarized spectra also yield a splitting of the $^4E(G)$-$^6A_1(S)$ peak [Fig. 8(e)]. Apparently, the splitting of the $^4E(G)$ state is too small to be resolved with a linewidth this large. Consequently, the $^4E(G)$ state splits at least into a doublet with a magnitude of 1.4 meV. However, further unresolved splitting cannot be ruled out, making conclusions about the Jahn-Teller coupling of the $^4E(G)$ state impossible. The $^4T_2(G)$-$^6A_1(S)$ absorption at 2.0172 eV has been intensively investigated by Heitz *et al.* using high-resolution PLE. A fourfold structure was resolved with the lowest transition at 2.0091 eV, indicating a weak Jahn-Teller coupling due to the hexagonal host lattice.[8]

7. Effective-mass-like state and charge-transfer level

A peak at 2.812 eV yields a strong phonon coupling which appears as a steplike structure and is indicated in Fig. 8(e). What Heitz *et al.* identified as a bound state consisting of an exciton bound to Fe^{3+} $[(Fe^{3+},e,h)]$ is in fact the first replica at 2.884 eV.[8] Table IV lists the replicas and possible candidates of their origin. By comparing the energies of phonon and local vibrational modes, there are three possible explanations for the most pronounced replicas with an energy between 72 and 73 meV: (i) The combination of two A_1 LVMs of 37.3 meV (Ref. 26) each is unlikely since the replica at this value is unequally weaker. (ii) An A_1 LVM of 75.10 meV (Ref. 27) and (iii) an E_2(high) phonon mode of 70.50 eV (Ref. 24) both deviate from the experimentally found value by about 2 meV. While the energy of the resonance between 37 and 38 meV (see Table IV) perfectly agrees with the A_1 LVM of 73.3 meV,[26] the origin of the replica at 24 meV is still unclear.

The steplike structure is the result of the bound state's replica superimposed on the start of a broad absorption band occurring in the UV spectral region. This band represents the $Fe^{3+/2+}$ CT process

$$Fe^{3+}(^6A_1(S)) + h\nu \rightarrow Fe^{2+} + h_{VB}, \quad (1)$$

in which a hole is excited into the valence band.[8] The CT band's low-energy onset equals the position of the $Fe^{3+/2+}$ CT level within the band gap as measured from the valence-band maximum. An exponential fit narrows it down to 2.863±5 eV. Heitz *et al.* could not accept this value, since it is below what they believed to be the bound state. Instead the CT level was thought to be at 3.17±0.1 eV.[8] The new position of the CT level brings the following implications upon the bound state: With the CT level further away from the CB 0.68±0.06 eV, only a minor hybridization of the Fe ion's core states with the CB needs to be taken into account. In addition, since the binding energy is only 50±10 meV, the hole is bound less tightly, producing a smaller overlap between the hole and core wave functions. Both effects lead to a weak exchange interaction between the hole and core states. Consequently, the bound state is of the same character as the Fe acceptor in other III-V materials, which is best described as a hole bound to an Fe^{2+} center (Fe^{2+},h_{VB}).[18,32,33]

This shallow bound state can be described as an effective-mass-like complex with a Coulomb interaction. It constitutes a transient shallow acceptor state and represents the highest excited state of the Fe^{3+} center. A bound state of the form (Fe^{2+},h_{VB}) would also explain the deviation from the LVM energy that was originally calculated and measured for the Fe^{3+} ground state.[27] As a result, the A_1 LVM discussed above is probably the cause of the replica with an energy between 72 and 73 meV.

High-resolution transmission spectra of the 2.812-eV line (not shown here) yield a threefold splitting of a magnitude of approximately 8 meV. This observation is in good agreement with findings in GaAs, GaP, and InP where the core wave functions, though influenced by the loosely bound hole, are well localized at the Fe^{2+} ion.[18,32,33] Consequently, the fine structure of the $Fe^{2+}(^5E)$ state is indicated by the observed splitting. In fact, the ^5E state of cubic lattice types bears five sublevels. However, even in high-resolution calorimetric absorption spectroscopy of Fe-doped InP and GaP only three lines are well resolved.[32]

Under the influence of the axial distortion of the tetrahedral crystal field (C_{3V} symmetry) the $Fe^{2+}(^5E)$ state is shown to further split into at least seven sublevels.[13] Apparently, only three of those are resolved in form of the fine structure of the bound state. The factor between the splitting observed here and the splitting of the $Fe^{2+}(^5E)$ state is roughly 2, which agrees with findings for the same state in InP and GaP.[13,32]

Figure 9 shows a transmission spectrum which was recorded with the c axis parallel to the optical path, resulting in an absorption path length of 400 μm. Besides the discussed effective-mass-like state at 2.812 eV, it shows another absorption feature of multifold structure around 3.127 eV. In analogy to the 2.812-eV peak representing a hole bound to the Fe^{2+} ground state, ^5E, we tentatively assign this feature to a hole bound to the excited state of Fe^{2+}, $^5T_2$. Equivalent transitions have been identified successfully for Fe^{2+} in GaAs, GaP, and InP.[18,34,35] The assumption is supported by the observed splitting, reflecting the fine structure of the

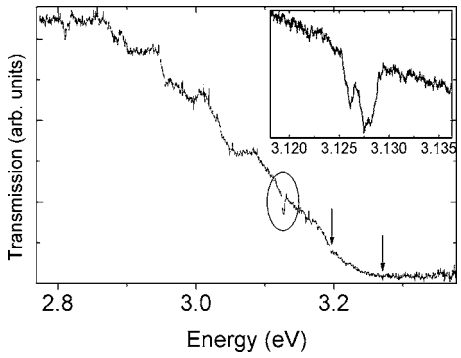

FIG. 9. Optical UV transmission spectrum of GaN with [Fe] $=1\times10^{19}$ cm^{-3} at 2 K and $\vec{k}\|c$ axis. A sharp absorption feature is detected peaking around 3.127 eV. The arrows indicate possible phonon replicas of ~72 meV. The inset shows a high-resolution spectrum of the encircled area.

$Fe^{2+}(^5T_2)$ state and by the steps in Fig. 9 at 3.1974 and 3.2707 eV (arrows). As with the $(Fe^{2+}(^5E),h_{VB})$ state, the latter are the replicas on account of the discussed A_1 LVM or E_2(high) phonon mode with an energy of 73 meV. The spacing between the two discussed bound states amounts to 315 meV. However, the energy of the $^5E\rightarrow{}^5T_2$ transition of the ^5D states of Fe^{2+} is shown to be 385 meV later on in this work. As a result, the binding energy of the effective-mass-like state involving the excited ^5E state of Fe^{2+} would have a 70 meV higher binding energy than the one discussed before. For the host materials GaAs, GaP, and InP these respective energies are equal.[18,34,35] Therefore, it is possible that the peak at 3.1275 eV is caused by impurities originating from the substrate. This assumption is supported by the fact that the absorption line at 3.1275 eV was only detected for the light traveling parallel to the *c* axis.

In summary, all absorption features found by VIS-UV transmission experiments (Fig. 8) were assigned to internal transitions within the Fe^{3+} center. Since none of those features was observed for a Fe concentration of 5×10^{17} cm^{-3} [Fig. 8(a)], it can be concluded that at this concentration no Fe ions are present in the 3+ charge state. The cause is the position of the Fermi level above the $Fe^{3+/2+}$ CT level. As discussed above, only with increased Fe concentration residual *n*-type conductivity is compensated by Fe acceptors, eventually lowering the Fermi level deep enough for Fe^{3+} centers to stay un-ionized. Consequently, the Fe^{3+} luminescence in Fig. 2(a2) for low Fe concentrations must be excited via a different channel than intracenter transitions.

8. Term scheme of Fe^{3+}

Figure 10 illustrates the term scheme of Fe^{3+} in GaN on the basis of the just outlined findings rectifying the one established by Heitz *et al.*[8] The most important points are the position of the CT level at 2.863 eV±5 meV above the valence band and the binding energy of the pseudoacceptor (Fe^{2+},h_{VB}) of (50±10) meV. The implications of the position of the CT level regarding the applicability of the internal reference rule[6,7] for the prediction of band offsets in semiconductor heterojunctions (HJ's) are the following: For the

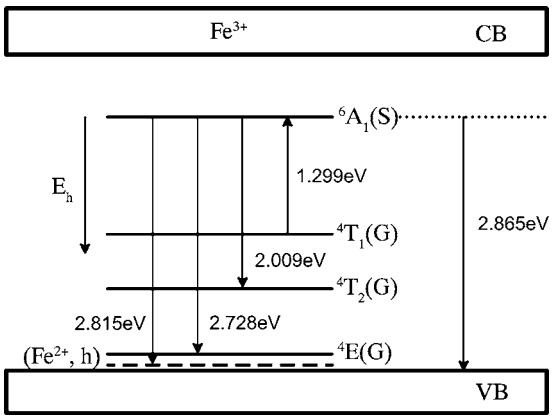

FIG. 10. Term scheme of Fe^{3+} in GaN. The ^4G state is split by the crystal field into the ground state $^6A_1(S)$ and the excited states $^4T_1(G)$, $^4T_2(G)$, and $^4E(G)$. Further excitation leads to a shallow bound state (binding energy of 50±10 meV). Transitions between these states are described best in the hole picture as indicated by the arrow on the left-hand side. Transitions observed in transmission experiments are indicated by arrows.

GaN/GaAs HJ, a valence-band discontinuity of 1.84±0.1 eV has been established by ultraviolet photoemission spectroscopy and first-principles calculations.[36,37] However, our results suggest a type-I band alignment with a valence-band offset of 2.4 eV. Obviously, the internal reference rule cannot be used to predict band discontinuities between GaN and other III-V materials. The reason probably relates to the exceptionally large electronegativity of nitrogen in comparison to other group-V elements.

No conclusion about the validity of the internal reference rule for the GaN/AlN material system can be drawn. By means of x-ray photoemission spectroscopy a type-I lineup with a valence-band discontinuity of 0.7±0.24 eV has been found.[38] However, the only literature about the $Fe^{3+/2+}$ level in AlN is based on an inaccurate experimental methodology, which results in a large experimental error.[20] Assuming the internal reference rule holds for the GaN/AlN HJ, our results suggest the CT level in AlN to be 2.6 eV below the conduction band.

An additional consequence of the $Fe^{3+/2+}$ CT level being located 0.68±0.06 eV below the conduction band is that the $Fe^{2+}((^5E\rightarrow{}^5T_2))$ transition might be located within the band gap. This transition was previously believed to be absent, since the CT level was thought to be 0.33 eV below the conduction band and, with typical $^5E\rightarrow{}^5T_2$ transition energies of 0.35–0.40 eV, the $^5T_2$ level might degenerate with the conduction band. Indeed, in agreement with the deeper $Fe^{3+/2+}$ CT level, the existence of the $Fe^{2+}((^5E\rightarrow{}^5T_2))$ transition could be shown by IR transmission experiments as illustrated in the following section.

B. Fe^{2+} center

In Fig. 11(b), FTIR spectra of the set of Fe-doped GaN samples exhibit a richly structured absorption band at around 395 meV. We assign this feature to the internal ^5E-$^5T_2$ transition of Fe^{2+} on the basis of three reasons: (i) The observed

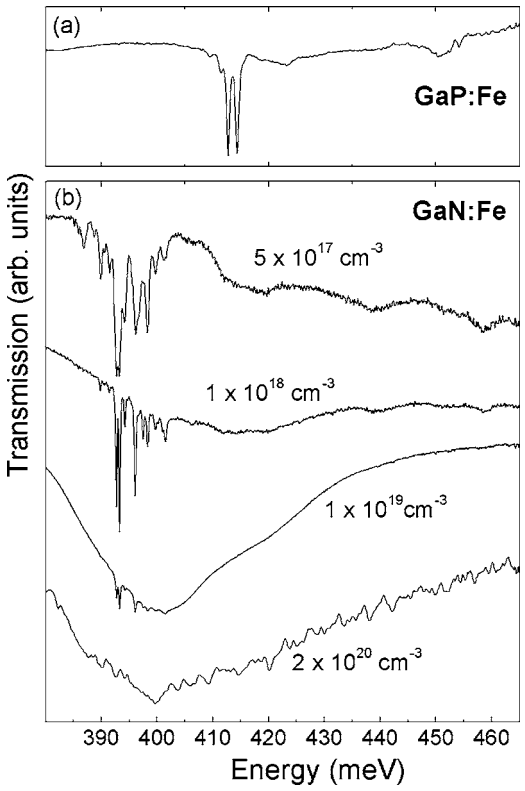

FIG. 11. FTIR transmission spectra of (a) Fe-doped GaP and (b) Fe-doped GaN showing the richly structured $Fe^{2+}({}^5E \rightarrow {}^5T_2)$ transition in both materials at $T \approx 40$ K. The noisy signal for [Fe]=2 $\times 10^{20}$ cm^{-3} is the result of the very high overall absorption of this sample.

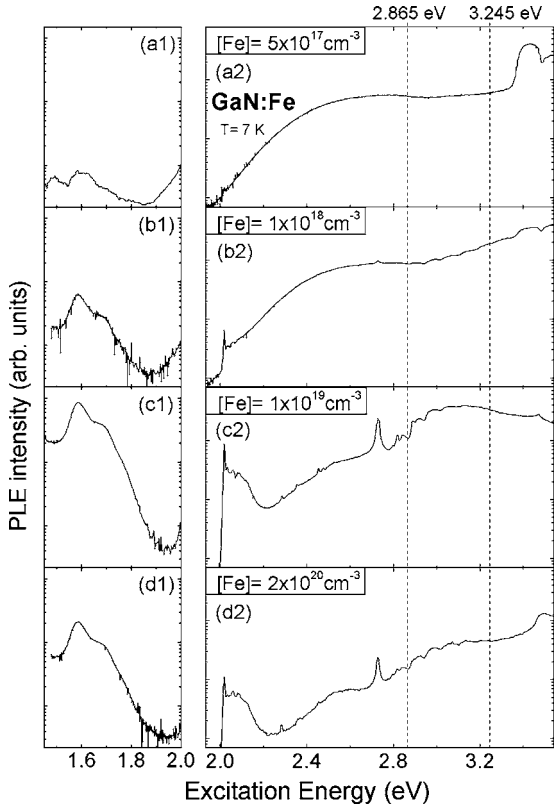

FIG. 12. PLE spectra of the $Fe^{3+}({}^4T_1(G) \rightarrow {}^6A_1(S))$ luminescence at 1.299 eV of Fe-doped GaN at 7 K on logarithmic scale. The luminescence was detected in an 8-meV-wide window around 1.299 eV. All spectra in one column are displayed on the same intensity scale. The dashed lines mark the onsets of excitation bands representing CT processes resulting in the Fe^{2+} states ${}^5E$ and ${}^5T_2$.

absorption structure is found in the same energetic region and is of similar shape as the same transition in GaAs, GaP, and InP—i.e., between 340 and 450 meV.[12] For comparison, the spectrum of the ${}^5E \rightarrow {}^5T_2$ transition in GaP recorded by the same experimental setting is displayed in Fig. 11(a). (ii) The shape and amplitude of the absorption changes significantly with the Fe concentration. (iii) PLE spectra presented below yield a second CT band at a distance from the first one equal to the position of the absorption feature in question.

The Fe^{2+} ion represents a d^6 configuration. In the trigonal ligand field of T_d symmetry in a cubic (zinc-blende) host lattice, the ${}^5D$ ground state splits into a ${}^5E$ ground state and a ${}^5T_2$ excited state. Spin-orbit interaction causes the ${}^5E$ and ${}^5T_2$ states to split into five and six sublevels, respectively. This splitting can be used to explain the GaP:Fe^{2+} spectrum in Fig. 11(a), taking into account a strong Jahn-Teller coupling and the thermal population of the ground states as well as selection rules.[12,33,39] The spectra of the ${}^5E$-${}^5T_2$ transition in GaN [Fig. 11(b)] are more complex because of an additional splitting due to the axial distortion of the crystal field in C_{3V} symmetry. The precise assignment of the observed transitions and the determination of the Fe^{2+}-term scheme will be presented in a separate paper.[13] We have observed a similar transition in Fe-doped ZnO, which is currently the topic of further study.

With increasing Fe concentration, a broad absorption band develops at the position of the Fe^{2+} transitions at around 400 meV that probably results from an intercenter interaction that causes the single ${}^5E \rightarrow {}^5T_2$ lines to broaden.

Since the ${}^5E \rightarrow {}^5T_2$ transition is present in all spectra of Fig. 11(b), we can assume that Fe^{2+} is a stable charge state at any Fe concentration. A dynamic process in which Fe^{2+} is only created from present Fe^{3+} can be ruled out because the specimens were not exposed to light of sufficient energy (2.865 eV) to accomplish the $Fe^{3+/2+}$ charge-transfer process. Consequently, we conclude that the Fermi level does not drop below the $Fe^{3+/2+}$ charge-transfer level at 2.865 eV, leading to a coexistence of Fe^{3+} and Fe^{2+} at high Fe concentrations.

As mentioned before, Fe^{2+} was not detected by EPR. A possible explanation for this discrepancy between optical and magnetic experiments is the fact that Fe^{2+} (d^6 configuration) is a non-Kramers ion and therefore difficult to detect by EPR.

C. Excitation processes

In order to gain further insights into the excitation and CT processes in Fe-doped GaN, PLE studies of the $Fe^{3+}({}^4T_1(G) \rightarrow {}^6A_1(S))$ luminescence were conducted. The detection window was set to an 8-meV-wide window around 1.299 meV. Figure 12 illustrates PLE measurements for dif-

ferent Fe concentrations. The spectra show similar features to those observed in transmission experiments: Internal transitions into the excited Fe^{3+} states $^4T_2(G)$ and $^4E(G)$ and the effective-mass-like state for Fe concentrations from 1×10^{18} cm^{-3}. The vibronic sideband of the $^4T_2(G)$ transition was analyzed in detail by Heitz *et al.* and indicates a dynamic Jahn-Teller effect.[8] The presence of the $Fe^{3+/2+}$ CT band starting at 2.865 ± 0.008 meV suggests that the CT process initiates a very efficient excitation mechanism of the Fe^{3+} center. This excitation process is described in detail by the following equation:

$$Fe^{2+} + h_{VB} \rightarrow (Fe^{2+}, h_{VB}) \xrightarrow{nonrad.} Fe^{3+}(^4T_1). \qquad (2)$$

Following the $Fe^{3+/2+}$ CT process [Eq. (1)] the free hole is captured by an Fe^{2+} center probably by first forming the discussed bound (Fe^{2+}, h_{VB}) state, which then relaxes nonradiatively into the $Fe^{3+}(^4T_1(G))$ state. The position of the CT band observed here is in good agreement with the results of the transmission spectra (Fig. 8). A second excitation band can be seen, particularly for $[Fe]=2\times10^{20}$ cm^{-3} in Fig. 12(d2), starting at 3.245 ± 0.02 eV. The difference between the two onsets, 380 ± 20 meV, equals the splitting of the ^5D state of Fe^{2+} established by FTIR measurements. Consequently, the second band represents the CT process resulting in the Fe^{2+} state, $^5T_2$.

The spectra presented in Figs. 12(b2)–12(d2) suggest that the capture of free holes by Fe^{2+} centers is the most efficient excitation mechanism of Fe^{3+}. GaN samples with Fe concentrations of 1×10^{18} cm^{-3} and 5×10^{17} cm^{-3} exhibit weak or no Fe^{3+}-related features, respectively. Nevertheless, they show the Fe^{3+} luminescence at the same intensity as higher-doped samples and, according to FTIR experiments, they definitely contain Fe^{2+}. Therefore, at low Fe concentrations, holes must be provided via different channels. Excitation processes of the Fe^{3+} luminescence by hole transfer from other impurities to Fe^{2+} centers are known from *n*-type II-VI semiconductors—e.g., ZnO and ZnS.[16,19] In ZnS, Cu^{2+} is a well-established source of free holes.[16] By means of PLE and two color stimulation, Hoffmann *et al.* established a close correlation between the excitation processes of the Fe^{3+} center and the intrinsic yellow luminescence (YL) of *n*-type GaN.[40] According to Ref. 40, the ionization of natural defects forming deep double donors around 2.3 eV below the CB initiates the YL transition and, at the same time, represents the first step of a two-step generation of free holes.[41] PLE spectra of the YL yield the ionization process in form of the same excitation band starting at 2.1 eV as presented in Fig. 12.[40] Hence, the deep defects involved in the yellow luminescence can act as a hole source equally at any investigated Fe concentration, as the 2.1-eV band is present with equal intensity in all spectra of Fig. 12. Consequently, the quenching of the YL by the incorporation of iron[42] is merely accomplished by the lowered Fermi level, ionizing the shallow donor involved in the YL.[41] That also explains the equal intensity of the Fe^{3+} luminescence in Fig. 2 which was excited at 2.4 eV, where the dominating excitation process is the generation and subsequent capture of holes as outlined above. Apparently, the bottleneck of the Fe^{3+} excitation at this energy is not the density of Fe centers but the availability of hole sources (i.e., intrinsic deep defects) which is shown here to be independent of the Fe doping. The observation of the 2.1-eV band in all spectra presented in Fig. 12 also confirms the presence of Fe^{2+} even at high Fe concentrations in agreement with the FTIR spectra (Fig. 11) and the position of the Fermi level.

The near-band-gap excitation at 3.4 eV [Figs. 12(a2) and 12(b2)] is tentatively explained by a hole generation via the shallow donor state 35 meV below the CB involved in the YL.[40] This donor would be passivated at higher Fe concentrations.

The positions of the sharp minima at 3.484 eV for $[Fe]=5\times10^{17}$ cm^{-3} and 1×10^{18} cm^{-3} and maxima at 3.472 eV for $[Fe]=1\times10^{19}$ cm^{-3} and 2×10^{20} cm^{-3} (broadened) coincide with the values of free and bound excitons found for 400-μm-thick HVPE-grown GaN on sapphire.[14] Consequently, energy resulting from the bound exciton recombination is transferred to Fe^{3+} centers present at high Fe concentrations contributing to the Fe^{3+} luminescence. On the other hand, the recombination of the free exciton represents a competing process. A strong competition between the recombination via the free exciton and via the Fe^{3+} center was reported for ZnO.[19]

The spikes superimposed on the spectra of high Fe concentrations between 2.3 and 2.4 eV are attributed to internal transitions of Fe-related complexes, implying that despite a careful choice of detection window, the defect luminescence (Fig. 6) was also detected. PLE spectra of the line at 1.268 eV yield an excitation band at the same position.[29] Considering the capture of free holes to be the most efficient excitation process of the Fe^{3+} luminescence, such defect luminescence is likely to represent competing recombination channels.

Finally, we observe an excitation band with peaks at 1.6 and 1.65 eV which clearly scales with the Fe concentration up to 1×10^{19} cm^{-3} [see Figs. 12(a1)–12(d1)]. Its origin is still unclear. A possible interpretation is a generation of free holes via defects involved in the red luminescence (RL) occurring in GaN around 1.9 eV,[43,44] similar to the mechanism described above for the YL defects.

IV. CONCLUSION

In this paper, the structural, optical, and electronic properties of GaN doped with different concentrations of Fe were investigated. A good crystal quality and a strain-free incorporation of Fe on Ga site was proven by the EPR signal of Fe^{3+}, by the small FWHM of the $^4T_1(G)\rightarrow{}^6A_1(S)$ luminescence, and by the concentration-independent energy of the E_2(high) phonon mode. Fe was observed in the charge states 3+ and 2+ by optical experiments. The respective electronic structures were established. For Fe^{3+}, besides the $^6A_1(S)$ ground state and the excited states $^4T_1(G)$, $^4T_2(G)$, and $^4E(G)$, an effective-mass-like state consisting of a hole bound to Fe^{2+} (Fe^{2+}, h_{VB}) was established as the highest excited state of Fe^{3+}. With a binding energy of 50 ± 10 meV it represents a shallow transient acceptor state very similar to the same phenomenon in cubic III-V materials. While the

fine structure of the $Fe^{3+}(^4T_1(G))$ state could be successfully established, we can only report the existence of a splitting for the $^4E(G)$ state ($\sim$1.4 meV) and the effective-mass-like state ($\sim$8 meV for both Fe^{2+} states). The fine structure of the latter reflects the splitting of the Fe^{2+} state involved in the bound state. For Fe^{2+}, we observed the internal $^5E \rightarrow {}^5T_2$ transition at all studied Fe concentrations with the splitting of the ^5D state amounting to 385 meV. Effective-mass-like complexes were observed involving both the ^5E and $^5T_2$ states of Fe^{2+}, 2.812 eV and 3.127 eV above the Fe^{3+} ground state, respectively. The $Fe^{3+/2+}$ charge-transfer level was determined to be 2.863 ± 0.005 meV above the VB maximum. On the basis of this value, we conclude, that the internal reference rule does not hold for GaN in conjunction with other III-V materials. No conclusion could be made regarding the heterojunction with AlN.

We found a strong coupling of internal Fe^{3+} transitions on E_2 phonon modes and A_1 and E LVMs. In contrast to cubic II-VI and III-V host materials, only a weak Jahn-Teller interaction effects the electronic states of both charge states. The reason is probably the reduced ligand-field symmetry in C_{3V} configuration. At Fe concentrations from 1×10^{19} cm^{-3}, defect complexes involving Fe are formed which cause additional PL and EPR lines. The vibrational coupling is similar to that of isolated Fe centers. $Fe_{Ga}{}^{3+}$-Ga_i pairs were identified by angular-dependent EPR. A very efficient excitation process for Fe^{3+} was proven to be the capture of free holes by Fe^{2+} centers. The holes are generated in a CT process from Fe^{3+} or in a two-step process via the intrinsic shallow donor and the deep double donor involved in the YL. The results of our optical experiments suggest that Fe^{2+} is present at all studied Fe concentrations, whereas Fe^{3+} only seems to exist at higher concentrations from 1×10^{18} cm^{-3}. Consequently, at these high concentrations, electron trapping by the Fe acceptor has lowered the Fermi level close to the $Fe^{3+/2+}$ CT level, compensating intrinsic n-type conductivity. For higher Fe contents the Fermi level does not drop below the CT level but instead stays pinned to it, leading to a coexistence of Fe^{3+} and Fe^{2+}.

ACKNOWLEDGMENTS

Financial support from the Australian Research Council is gratefully acknowledged.

*Corresponding author. Present address: Microstructural Analysis Unit, University of Technology, Sydney, Australia. Electronic address: Malguth@physik.tu-berlin.de

†Present address: WS Materials Technology, LLC, 15 Central St., Stamford, CT 06906, USA.

[1] B. Monemar and O. Lagerstedt, J. Appl. Phys. **50**, 6480 (1979).

[2] R. P. Vaudo, X. Xu, A. Salant, J. Malcarne, and G. R. Brandes, Phys. Status Solidi A **200**, 18 (2003).

[3] M. S. Shur and M. A. Khan, in *GaN and AlGaN Devices: Field Effect Transistors and Photodetectors*, edited by S. J. Pearton (Gordon and Breach, Amsterdam, 2000), pp. 47–92.

[4] T. Graf, S. T. B. Goennenwein, and M. S. Brandt, Phys. Status Solidi B **239**, 277 (2003).

[5] H. Ohno, Science **281**, 951 (1998).

[6] J. M. Langer and H. Heinrich, Phys. Rev. Lett. **55**, 1414 (1985).

[7] J. M. Langer, C. Delerue, M. Lannoo, and H. Heinrich, Phys. Rev. B **38**, 7723 (1988).

[8] R. Heitz, P. Maxim, L. Eckey, P. Thurian, A. Hoffmann, I. Broser, K. Pressel, and B. K. Meyer, Phys. Rev. B **55**, 4382 (1997).

[9] K. Maier, M. Kunzer, U. Kaufmann, J. Schneider, B. Monemar, I. Akasaki, and H. Amano, Mater. Sci. Forum **143-147**, 93 (1994).

[10] J. Baur, K. Maier, M. Kunzer, U. Kaufmann, J. Schneider, H. Amano, I. Akasaki, T. Detchprohm, and K. Hiramatsu, Appl. Phys. Lett. **64**, 857 (1994).

[11] R. Heitz, P. Thurian, I. Loa, L. Eckey, A. Hoffmann, I. Broser, K. Pressel, B. K. Meyer, and E. N. Mokhov, Appl. Phys. Lett. **67**, 2822 (1995).

[12] L. Podlowski, R. Heitz, P. Thurian, A. Hoffmann, and I. Broser, J. Lumin. **48**, 252 (1994).

[13] E. Malguth, A. Hoffmann, and X. Xu, preceding paper, Phys. Rev. B **74**, 165201 (2006).

[14] B. K. Meyer, A. Hoffmann, and P. Thurian, in *Group III Nitride Semiconductor Compounds*, edited by B. Gil (Clarendon Press, Oxford, 1998), pp. 242–306.

[15] W. Gehlhoff, D. Azamat, U. Haboeck, and A. Hoffmann, in *Condensed Matter Proceedings of the 23rd International Conference on Defects in Semiconductors*, edited by A. Oshiyama, K. Maeda, K. M. Itoh, and H. Katayama-Yoshida [Physica B **376-377**, 486 (2006)].

[16] A. Hoffmann, R. Heitz, and I. Broser, Phys. Rev. B **41**, 5806 (1990).

[17] K. Pressel, G. Bohnert, G. Ruckert, A. Dornen, and K. Thonke, J. Appl. Phys. **71**, 5703 (1992).

[18] K. Pressel, A. Dörnen, G. Rückert, and K. Thonke, Phys. Rev. B **47**, 16267 (1993).

[19] R. Heitz, A. Hoffmann, and I. Broser, Phys. Rev. B **45**, 8977 (1992).

[20] J. Baur, K. Maier, M. Kunzer, U. Kaufmann, and J. Schneider, Appl. Phys. Lett. **65**, 2211 (1994).

[21] P. Thurian and A. Hoffmann, in *Proceedings of the XIV International Symposium on Electron-Phonon Dynamics and Jahn-Teller-Effect, Erice, Italy, 1998*, edited by G. Bevilacqua, L. Martinelli, and N. Terzi (World Scientific, Singapore, 1998), pp. 216–229.

[22] K. Pressel, S. Nilsson, R. Heitz, A. Hoffmann, and B. K. Meyer, J. Appl. Phys. **79**, 3214 (1996).

[23] J. Baur, U. Kaufmann, M. Kunzer, J. Schneider, H. Amano, I. Akasaki, T. Detchprohm, and K. Hiramatsu, Appl. Phys. Lett. **67**, 1140 (1995).

[24] H. Siegle, L. Eckey, A. Hoffmann, C. Thomsen, B. K. Meyer, D. Schikora, M. Hankeln, and K. Lischka, Solid State Commun. **96**, 943 (1995).

[25] V. Y. Davydov, Y. E. Kitaev, I. N. Goncharuk, A. N. Smirnov, J. Graul, O. Semchinova, D. Uffmann, M. B. Smirnov, A. P. Mirgorodsky, and R. A. Evarestov, Phys. Rev. B **58**, 12899 (1998).

[26] P. Thurian, G. Kaczmarczyk, H. Siegle, R. Heitz, A. Hoffmann, I.

Broser, B. K. Meyer, R. Hoffbauer, and U. Scherz, Mater. Sci. Forum **196-201**, 1571 (1995).
[27] C. Goebel, C. Schrepel, U. Scherz, P. Thurian, G. Kaczmarczyk, and A. Hoffmann, Mater. Sci. Forum **258-263**, 1173 (1997).
[28] F. Demangeot, J. Frandon, M. A. Renucci, O. Briot, B. Gil, and R. L. Aulombard, Solid State Commun. **100**, 207 (1996).
[29] P. Thurian *et al.*, in *III-V Nitrides*, edited by F. A. Ponce, T. D. Moustakas, I. Akasaki, and B. A. Monemar, MRS Symposia Proceedings No. 449 (Materials Research Society, Pittsburgh, 1997), pp. 707–712.
[30] W. Gehlhoff, D. Azamat, and A. Hoffmann, Phys. Status Solidi B **243**, 1687 (2006).
[31] U. W. Pohl, H.-E. Gumlich, and W. Busse, Phys. Status Solidi B **125**, 773 (1984).
[32] L. Podlowski, R. Heitz, T. Wolf, A. Hoffmann, D. Bimberg, I. Broser, and W. Ulrici, Mater. Sci. Forum **143-147**, 311 (1994).
[33] K. Pressel, G. Rückert, A. Dörnen, and K. Thonke, Phys. Rev. B **46**, 13171 (1992).
[34] A. Juhl, A. Hoffmann, D. Bimberg, and H. J. Schulz, Appl. Phys. Lett. **50**, 1292 (1987).
[35] K. Thonke and K. Pressel, Phys. Rev. B **44**, 13418 (1991).
[36] S. A. Ding, S. R. Barman, K. Horn, H. Yang, B. Yang, O. Brandt, and K. Ploog, Appl. Phys. Lett. **70**, 2407 (1997).
[37] B. K. Agrawal, S. Agrawal, and R. Srivastava, Surf. Sci. **424**, 232 (1999).
[38] G. Martin, A. Botchkarev, A. Rockett, and H. Morkoc, Appl. Phys. Lett. **68**, 2541 (1996).
[39] G. Rückert, K. Pressel, A. Dörnen, K. Thonke, and W. Ulrici, Phys. Rev. B **46**, 13207 (1992).
[40] A. Hoffmann *et al.*, Solid-State Electron. **41**, 275 (1997).
[41] D. M. Hofmann, D. Kovalev, G. Steude, B. K. Meyer, A. Hoffmann, L. Eckey, R. Heitz, T. Detchprom, H. Amano, and I. Akasaki, Phys. Rev. B **52**, 16702 (1995).
[42] CL studies of the same set of GaN:Fe samples show that the yellow luminescence is significantly quenched with increasing Fe concentration.
[43] E. M. Goldys, M. Godlewski, T. Paskova, G. Pozina, and B. Monemar, MRS Internet J. Nitride Semicond. Res. **6**, 1 (2001).
[44] In CL spectra we observed the RL with a similar shape and position as in the present PLE studies.